HHS Public Access

Author manuscript

Nat Neurosci. Author manuscript; available in PMC 2011 March 01.

Published in final edited form as:

Nat Neurosci. 2010 September ; 13(9): 1090–1097. doi:10.1038/nn.2621.

Narp regulates homeostatic scaling of excitatory synapses on Parvalbumin interneurons

Michael C. Chang[1], **Joo Min Park**[1,5], **Kenneth A. Pelkey**[3,5], **Heidi L. Grabenstatter**[4,5], **Desheng Xu**[1], **David J. Linden**[1], **Thomas P. Sutula**[4], **Chris J. McBain**[3], and **Paul F. Worley**[1,2]

[1]The Solomon H. Snyder Department of Neuroscience, The Johns Hopkins University School of Medicine, Baltimore, MD

[2]Department of Neurology, The Johns Hopkins University School of Medicine, Baltimore, MD

[3]Laboratory of Cellular and Synaptic Neurophysiology, *Eunice Kennedy Shriver* National Institute of Child Health and Human Development, National Institutes of Health, Bethesda, MD

[4]Department of Neurology, University of Wisconsin, Madison, WI

Abstract

Homeostatic synaptic scaling alters the strength of synapses to compensate for prolonged changes in network activity, and involves both excitatory and inhibitory neurons. The immediate-early gene termed *Narp* (Neuronal activity-regulated pentraxin) encodes a secreted synaptic protein that can bind and cluster AMPA receptors (AMPARs). Here, we report that Narp prominently accumulates at excitatory synapses on Parvalbumin-expressing interneurons (PV-INs). Increasing network activity results in a homeostatic increase of excitatory synaptic strength onto PV-INs that increases inhibitory drive, and this response is absent in neurons cultured from *Narp* knock-out (*Narp*$^{-/-}$) mice. Activity-dependent changes in the strength of excitatory inputs on PV-INs in acute hippocampal slices are also dependent on Narp, and *Narp*$^{-/-}$ mice display increased sensitivity to kindling-induced seizures. We propose that Narp recruits AMPARs at excitatory synapses onto PV-INs to rebalance network excitation/inhibition dynamics following episodes of increased circuit activity.

Introduction

Long-lasting changes in synaptic strength underlie information storage within the central nervous system. Within the hippocampus, Hebbian long-term potentiation (LTP) and long-term depression (LTD) provide neurons with an effective use-dependent means for modification of individual synapses. However, the positive feedback nature of these

[5]These authors contributed equally to this work

Author Contributions: M.C.C. designed the experiments, carried out the *in vitro* immunocytochemical and biochemical studies and analysis and wrote the bulk of the manuscript. J.M.P. performed the *in vitro* electrophysiological experiments and analysis and contributed to the manuscript. K.A.P performed the slice electrophysiological experiments and analysis and contributed to the manuscript. H.L.G. performed the kindling experiments and analysis and contributed to the manuscript. D.X. provided reagents and helped with the discussion. P.F.W., D.J.L, T.P.S., and C.J.M directed the project.

processes makes them inherently unstable[1]. Additionally, for LTP or LTD to occur, basal synaptic strength must be maintained within an optimal range to prevent occlusion of further increases or decreases in activity[2], [3]. Therefore, bidirectional homeostatic feedback mechanisms are critical to provide long-term stability of networks and to ensure their potential for plasticity.

Immediate-early genes (IEGs) are dynamically regulated by forms of synaptic activity that underlie information processing and storage, making them excellent candidates to contribute to both Hebbian and homeostatic plasticity. For example, Activity-regulated cytoskeleton-associated protein (*Arc*, also known as *Arg3.1*) is a cytosolic protein that associates with Endophilin and Dynamin and increases the rate of endocytosis of AMPA receptors (AMPARs) at synapses on pyramidal neurons[4]. Steady state levels of Arc increase or decrease in parallel with changes in neuronal activity and contributes to bidirectional control of homeostatic scaling of AMPAR on pyramidal neurons[5]. Arc also contributes to synapse-specific mGluR-LTD in a process that involves the rapid *de novo* translation of *Arc* mRNA[6].

Neuronal activity-regulated pentraxin (*Narp*, also known as *Neuronal pentraxin 2*) is another IEG that can alter synaptic function. Narp is a member of the neuronal pentraxin (NP) family of calcium-dependent lectins that includes Neuronal pentraxin 1 (NP1) and Neuronal pentraxin receptor (NPR)[7]. Of these, only *Narp* is regulated as an IEG[8]. Narp and NP1 are secreted proteins, while NPR possesses an N-terminal transmembrane domain[9]. On the extracellular surface, these NPs form large, organized heteromeric complexes, stabilized via disulfide bond linkages[8]. NPs localize to excitatory synapses where their conserved, C-terminal pentraxin domains can interact with the N-terminal extracellular domain of AMPARs[10]. These features underlie the contribution of NPs in various forms of synaptic plasticity. For example, axonally derived NP1 and NPR are critical for the recruitment of AMPARs to both artificial and native synapses[10]. Additionally, NPR plays an essential role in mGluR-LTD in a process that involves activation of the extracellular metalloprotease TACE (TNF-α converting enzyme), cleavage of NPR near the transmembrane domain, and rapid endocytosis of NPR and AMPAR[11]. At the systems level, NPs are important for the activity-dependent segregation and refinement of eye-specific retinal ganglion cell projections to the dorsal lateral geniculate nucleus[12].

Here, we found that Narp was highly enriched at excitatory synapses present specifically on Parvalbumin-expressing interneurons (PV-INs) and its expression was dynamically regulated by network activity. Accumulation of Narp at these synapses resulted from its secretion from presynaptic excitatory neurons and required the presence of perineuronal nets surrounding PV-INs. Narp increased synaptic strength at PV-IN excitatory synapses, both in culture an in the acute hippocampal slice, by regulating levels of GluR4-containing AMPARs in an activity-dependent manner. Mice lacking Narp displayed a marked increase in sensitivity to kindling-induced seizure. Together, these results demonstrate that Narp contributes to homeostatic plasticity of interneurons and suggests a key role in the activity-dependent recruitment of PV-IN-mediated inhibition.

Results

Narp is enriched at excitatory synapses on PV-INs

We examined Narp protein expression by surface labeling primary hippocampal cultures prepared from embryonic day 18 (E18) mice after 14–17 days in vitro (DIV). Narp immunocytochemical (ICC) staining was markedly enriched on a small subpopulation of large neurons with complex dendritic branches (Fig. 1a). Lower levels of Narp were distributed broadly on the majority of neurons. Based on its expression pattern, we asked if Narp preferentially accumulated onto interneurons. Interneurons represented ∼10% of neurons within our hippocampal culture preparations and included distinct subtypes (unpublished observation). We performed ICC with antibodies against the calcium-binding proteins Parvalbumin (PV), Calretinin, and CAMKIIα, which represent non-overlapping neuronal subpopulations[13]. Pyramidal neurons expressing CAMKIIα, as well as Calretinin-expressing interneurons, displayed similar, low levels of Narp on the surface of their dendrites, while dendrites of PV-expressing interneurons (PV-INs) exhibited 10-fold higher levels of surface Narp (Fig. 1b,c). A similar enrichment of Narp was seen in PV-INs within the hippocampus *in vivo*. (Fig. 1d)

Narp is present at excitatory synapses on cultured spinal cord and hippocampal interneurons[14], [15]. To assess if Narp is at excitatory synapses on PV-INs, we labeled cultures with antibodies against Narp, Parvalbumin, and the excitatory synaptic scaffolding protein PSD95. Narp co-localized with PSD95, indicating that Narp localized to excitatory synapses on PV-INs (Fig. 1e). Narp did not co-localize with the inhibitory synaptic marker GAD65 (Supplementary Fig. 1).

While Narp expression is activity-regulated *in vivo*[7], we sought to confirm its activity-dependent expression in hippocampal cultures. ICC revealed that bicuculline treatment increased Narp protein levels ∼6-fold on PV-INs within 24 hours and ∼25-fold by 48 hours (Fig. 2a,b). Reciprocally, treatment of cultures with tetrodotoxin (TTX) led to an ∼50% reduction of Narp on PV-INs by 4 hours and an ∼80% decrease by 12 hours (Fig. 2a,b). Analysis by Western blot detected a prominent decrease in surface Narp in response to TTX, relative to control or bicuculline treatment (Fig. 2c,d). Bicuculline did not substantially increase surface Narp levels, consistent with the fact that PV-INs represent a small percentage of the total number of neurons, and that basal activity is high in the high density cultures used for biochemical analysis (Unpublished observation. Compare $\sim 1\times10^5$ cells/cm^2 for biochemistry vs $\sim 1.4\times10^4$ cells/cm^2 for immunocytochemistry. See methods). Consistent with previous results[7], [16], *Narp* mRNA levels also underwent activity-dependent changes (Fig. 2e).

Narp at PV-IN synapses derives from presynaptic neurons

To examine how Narp becomes enriched at excitatory synapses on PV-INs, we asked whether synaptic Narp is preferentially derived from pre- or postsynaptic neurons. Using a co-culture approach, we labelled a small number of either WT or *Narp*$^{-/-}$ neurons with CM-DiI and plated them amongst a much larger number of unlabeled neurons of the other genotype. CM-DiI is a water-soluble and fixable derivative of DiI, a non-toxic, lipophilic,

fluorescent dye that internalizes over time and persists in cultured neurons for up to 3.5 weeks[17]. When axons of presumed WT neurons contacted CM-DiI labeled *Narp*$^{-/-}$ PV-INs ("WT pre/$^{-/-}$ post"), Narp levels on *Narp*$^{-/-}$ interneurons were comparable to Narp levels on WT PV-INs within the same culture ("WT pre/WT post") (Fig. 3a,c). This suggests that a presynaptic source of Narp is sufficient for Narp accumulation at PV-IN excitatory synapses. Moreover, when presumed *Narp*$^{-/-}$ axons contacted CM-DiI labeled WT PV-INs ("$^{-/-}$ pre/WT post"), there was a significant reduction of Narp on PV-INs (Fig. 3b,c). The residual Narp present on these WT PV-Ins was not due to non-specific background since it was absent in *Narp*$^{-/-}$ cultures (data not shown), and instead could be attributed to postsynaptic secretion or to a small number of WT axons in the culture innervating these interneurons. The latter possibility is supported by the observation that *Narp*$^{-/-}$ PV-INs within the same culture ("$^{-/-}$ pre/$^{-/-}$ post") exhibited comparable levels of Narp on their dendrites. Taken together, these data indicate that Narp originates primarily from presynaptic neurons, consistent with previously published results[14], [15], [18].

Extracellular perineuronal nets enhance Narp accumulation

PV-INs comprise ~2.5% of the total neuronal population in our cultures (unpublished observation) and in the intact hippocampus[19]. Accordingly, excitatory synapses on PV-INs represent a small fraction of the total synapses in the culture, raising the question of how Narp could selectively accumulate at these synapses. One distinguishing trait of PV-INs is the presence of dense perineuronal nets, a specialized extracellular matrix consisting of chondroitin sulfate proteoglycans, glycoproteins, and glycosaminoglycans, which ensheath the soma, dendrites, and axon initial segment of PV-INs[20]. The polysaccharide side chains present on these molecules make them substrates for numerous plant-derived lectins including *Vicia villosa* agglutinin (VVA), *Wisteria floribunda* agglutinin, and soybean agglutinin[21], [22].

Because Narp is a calcium-dependent lectin[7], we speculated that these nets could provide a postsynaptic target to enhance accumulation of Narp. To test whether perineuronal nets play a role in Narp accumulation on PV-INs, we treated neuronal cultures with Chondroitinase ABC (ChABC), which degrades the glycosaminoglycan side chains of chondroitin sulfate proteoglycans and is used to disrupt perineuronal nets[23] (Supplementary Fig. 3). Treatment with ChABC for 48 hours led to a ~50% reduction in surface Narp levels on PV-INs (Fig. 4a,b). Even with addition of bicuculline, we found a significant reduction of surface Narp in cultures that were simultaneously treated with ChABC (Fig. 4b). ChABC did not reduce surface Narp detected by western blot (Fig. 4c,d), consistent with the notion that Narp at PV-INs represent a small fraction of the total secreted Narp that is also present at lower levels on other neurons (Fig. 1b,c). Taken together, this suggests that surface Narp expression still occurs in the presence of ChABC. However, Narp is unable to accumulate onto PV-INs in the absence of perineuronal nets.

Narp regulates GluR4 levels on PV-INs

Since Narp binds and clusters AMPARs[10], [15] and was highly enriched on PV-INs, we asked whether Narp could contribute to the regulation of either the GluR1 or GluR4 AMPAR subunits which PV-INs predominantly express[24]. A model in which *Narp*, an activity-

regulated gene, regulates AMPAR levels on PV-INs, predicts that AMPAR levels should scale in direct relation with network activity. To test this hypothesis, we treated neuronal cultures with either TTX or bicuculline, prior to staining for AMPARs. Bicuculline treatment resulted in a two-fold increase in PV-IN GluR4 levels by 48 hours, while TTX resulted in a 65% decrease (Fig. 5a,b). The kinetics for these activity-dependent changes in GluR4 followed that of Narp, where increases in GluR4 levels progressed much slower than reductions (Fig. 5d). GluR4 levels from untreated *Narp*$^{-/-}$ PV-INs were ∼50% lower than WT and failed to change in response to perturbations in activity (Fig. 5b,c). In contrast, GluR1, GluR2, and the NMDA Receptor subunit NR1, were not significantly different between WT and *Narp*$^{-/-}$ PV-INs (Supplementary Fig. 4).

Based on our finding that Narp accumulates on PV-IN synapses from presynaptic elements, we hypothesized that Narp from WT neurons might be sufficient to rescue GluR4 levels when deposited onto PV-INs lacking Narp. We tested this hypothesis by co-culturing WT and *Narp*$^{-/-}$ neurons and staining for GluR4. When we plated CM-DiI labeled *Narp*$^{-/-}$ PV-INs amidst surrounding WT neurons ("WT pre/$^{-/-}$ post"), we were able to partially rescue the reduced GluR4 levels on *Narp*$^{-/-}$ PV-INs (Fig. 5e,f). Importantly, when we reversed the genotypes and plated labeled WT PV-INs on surrounding unlabeled *Narp*$^{-/-}$ neurons ("$^{-/-}$ pre/WT post"), GluR4 levels were indistinguishable from *Narp*$^{-/-}$ PV-INs (Fig. 5f). In sum, these observations indicate that activity-dependent changes in Narp mediate parallel changes in GluR4 levels on PV-INs and implicate Narp in homeostatic scaling of these synapses.

Narp is required for homeostatic scaling of PV-INs

To evaluate how changes in total AMPAR levels functionally relate to synaptic strength, we performed patch clamp analysis of spontaneous miniature excitatory postsynaptic currents (mEPSCs). We initially identified PV-INs via live application of fluorescein-conjugated VVA and then confirmed their identity through their characteristic non-accommodating, fast-spiking response to current injection[25] (Supplementary Fig. 5a–c). Consistent with our ICC data, mEPSC amplitudes recorded from WT PV-INs changed in direct correlation with activity, and these changes were largely absent in *Narp*$^{-/-}$ PV-INs (Fig. 6a,b). In contrast, mEPSC frequency was not affected by changes in activity in either WT or *Narp*$^{-/-}$ PV-INs (Fig. 6c). Additionally, we found no changes in excitatory synapse number between WT and *Narp*$^{-/-}$ PV-INs as measured by double ICC labeling (Supplementary Fig. 6), indicating that PV-IN synaptogenesis proceeds independent of Narp. Together, these observations indicate that activity-dependent changes in Narp mediate parallel changes in synaptic strength of excitatory synapses on PV-INs and implicate Narp in homeostatic scaling of these synapses.

A model in which Narp regulates homeostatic adaptations of network activity via modulation of excitatory synapses on PV-INs predicts that the frequency of network-driven firing of PV-INs will be dependent on Narp. Accordingly, we compared spontaneous action potential frequency between WT and *Narp*$^{-/-}$ PV-INs. Consistent with our model, WT PV-INs spontaneously fired at more than double the rate of *Narp*$^{-/-}$ PV-INs (Fig. 6d,e). This difference was not attributable to changes in any membrane or action potential property we measured (Supplementary Fig. 7). Importantly, when we blocked synaptic transmission with gabazine, NBQX, and D-APV, we observed a complete elimination of action potentials (Fig.

6d), implying that all the spontaneous firing events were synaptically driven. These results suggest that the recruitment of GluR4 to excitatory synapses by Narp translates into increased activity of PV-INs.

Narp is critical for proper PV-IN function *in vivo*

To assess if the synaptic scaling deficit seen in *Narp*$^{-/-}$ cultures occurs in intact circuits *in vivo*, we examined excitatory input to PV-INs in acute hippocampal slices from WT and *Narp*$^{-/-}$ mice. We monitored spontaneous excitatory postsynaptic currents (sEPSCs) during whole-cell voltage clamp recordings from PV-INs situated in the dentate gyrus[26]. We initially selected presumptive PV-INs based on morphology and position at the dentate hilar border as well as fast-spiking properties. Then, we anatomically recovered and probed each recorded cell for PV expression, using biocytin processing combined with immunohistochemistry (Supplementary Fig. 5d,e). In contrast to cultured PV-INs, basal sEPSC amplitude and frequency were not significantly different between *Narp*$^{-/-}$ and WT PV-INs (Fig. 7). We hypothesized that this was due to low basal Narp levels in WT mice. Thus, in order to increase network activity, we administered maximal electroconvulsive seizure (MECS) to the mice ∼12–16 hours prior to obtaining slices for recording. Consistent with prior observations[15, 27], MECS significantly increased Narp levels in WT mice (Supplementary Fig. 8a). Moreover, in support of our working hypothesis, MECS administration to WT mice significantly increased the amplitude of sEPSCs recorded from PV-INs when compared to unstimulated controls (Fig. 7). This MECS-induced change was selective for PV-INs (Supplementary Fig. 8b–f) and was not associated with any other effects on sEPSC or firing properties examined (Fig 7b). We also probed hippocampal PV-IN GluR4 levels *in vivo* by immunohistochemistry and found a significant increase in GluR4 levels after MECS (Supplementary Fig. 9). Although the group average sEPSC kinetics did not change following MECS, we did observe the emergence of a negative correlation between sEPSC amplitude and decay time constant following MECS, consistent with recruitment of a fast GluR4-containing receptor population (Supplementary Fig. 10)[28]. Most importantly, MECS-induced plasticity of sEPSCs and GluR4 accumulation was absent in PV-INs from *Narp*$^{-/-}$ mice (Fig. 7 and Supplementary Figs. 9 and 10), confirming a role for Narp in activity-induced upregulation of excitatory input selectively onto PV-INs.

The importance of inhibitory networks in the suppression of seizures is well documented[29]. Thus, we hypothesized that the ability of Narp to regulate synaptic GluR4 levels on PV-INs, in response to activity, could be a compensatory mechanism for the suppression of epileptogenesis. To test this hypothesis, we stimulated awake, behaving 3–4 month old WT or *Narp*$^{-/-}$ mice twice daily in the basolateral amygdala and recorded the evoked afterdischarge (AD) from the same stimulating electrode. This stimulation protocol was sufficient to drive a significant increase of Narp protein expression in both the hippocampus and cortex of WT mice (Supplementary Fig. 11). With each evoked AD, we observed a gradual increase in seizure severity. We reached the first class III/IV seizures, in both WT and *Narp*$^{-/-}$ mice, after identical numbers of ADs. However, we began evoking more severe class V seizures after an average of 10 ADs in WT mice, while an average of only 6 ADs were required in *Narp*$^{-/-}$ mice (Fig. 8a). This difference was also evident in the number of ADs required to fully kindle the mice (i.e. evoke three class V seizures). Additionally, the

minimum current required to evoke an AD decreased more rapidly in *Narp*$^{-/-}$ mice, relative to WT mice, over the course of the experiment (Fig. 8b). These data suggest that Narp functions to inhibit kindling-evoked progression of circuits involved in the development of chronic and long-term seizure plasticity.

Discussion

Excitatory synapses onto PV-INs are capable of undergoing plasticity[30]-[32], and this study provides the first molecular mechanism for a postsynaptic form of plasticity at these synapses. Activity-dependent expression of Narp by presynaptic excitatory neurons regulates homeostatic adaptations of circuit activity by enhancing the strength of excitatory synapses on PV-INs, concomitantly increasing their network-driven firing rate. PV-INs are the most abundant subtype of interneuron within the hippocampus[19] and are implicated in processes such as gamma oscillations[33], visual cortical plasticity[34], and fear memory resilience[35]. Additionally, the dysfunction and/or loss of PV-INs may underlie several neurological disorders such as temporal lobe epilepsy[36] and schizophrenia[37]. Therefore, uncovering the molecular mechanisms of how these neurons regulate the strength of their synapses has implications for understanding plasticity and cognitive disorders.

The present model of Narp-dependent synaptic plasticity is consistent with its regulation as an IEG, and its ability to bind AMPARs and sugars[7], [15]. Increases in activity increase Narp expression in excitatory neurons and Narp is subsequently secreted, and preferentially accumulates, at excitatory synapses on PV-INs. Narp is required for activity-regulated changes in GluR4-mediated synaptic strength at these synapses. By this process, an IEG can evoke transsynaptic effects to modulate circuit activity. It is interesting to contrast the respective roles of *Narp* and *Arc* in homeostatic scaling. With sustained increases in activity, Arc is rapidly expressed and functions to promote the endocytosis and downregulation of GluR1 in pyramidal neurons[4], [5]. At the same time, Narp targets to PV-INs where it functions to cluster GluR4 and potentiate excitatory synapses on these neurons. Using independent mechanisms, *Narp* and *Arc* thereby function in a complementary manner, at two separate populations of glutamatergic synapses, to reset pyramidal neuron activity back to baseline levels.

Despite these molecular insights, several important questions arise. First, how is *Narp* expression regulated by activity? Recent evidence demonstrates that the activity-dependent transcription of *Narp* mRNA requires Ca^{2+} influx through L-type voltage-gated calcium channels (VGCCs) and subsequent activation of Ca^{2+}/calmodulin (CaM), CaM-dependent kinases, and Extracellular signal-regulated kinase (ERK) 1/2[38]. Additionally, *Narp* is misregulated by knockdown of the neuronal IEG transcription factor Npas4 via RNAi expression[39]. It is interesting to note that *Npas4*, and *Narp* share many similar features: both are activity-regulated genes, require Ca^{2+} influx through L-type VGCCs for their induction, are expressed primarily in excitatory neurons, and yet are both key regulators of the inhibitory network[39]. Whether Npas4 is required for Narp expression remains to be studied.

Second, how does Narp selectively accumulate on PV-INs? Glycoproteins appear to be important for the targeting of Narp to excitatory synapses on PV-INs, consistent with the

general property of pentraxins to bind sugars[40]. It is notable, however, that perineuronal nets are not localized precisely at synapses[41]. One model consistent with current data envisions that secreted Narp accumulates locally within the glycoprotein network, aided by lectin-based interactions. Narp might then diffuse along pre or postsynaptic membranes and localize to the synapse by interactions with other sugars or proteins, or form disulfide linked complexes with NPR[11]. The lectin properties of pentraxins are linked to the Ca^{2+} binding pocket, which in turn, is important for proper folding of the pentraxin domain[40]. Accordingly, it is difficult to selectively disrupt lectin properties by mutagenesis. Simple addition of recombinant Narp to cultures does not result in selective binding to PV-INs (unpublished observation), suggesting that targeting may involve processes beyond simple lectin-dependent binding.

Important questions also arise regarding how Narp can evoke an increase of GluR4, but not other AMPARs, on PV-INs. Binding of Narp to AMPARs does not require sugar adducts to the receptor, but rather, appears to be dependent on protein sequences within the N-terminal X-domain[10]. Previous reports demonstrate the capacity for NPs to bind and cluster AMPARs at sites of cell-cell contact[8], [9], [14]. It is possible that Narp-containing pentraxin complexes preferentially retain GluR4 on the cell surface, and this conjecture is consistent with the observation that NPs cluster homomeric AMPARs consisting of GluR4 subunits better than any other AMPAR subunit[9]. However, the avidity of Narp binding for GluR1 and GluR4 is not dramatically different in binding assays (unpublished observation) suggesting that the difference in activity-dependent accumulation may be due to factors in addition to their association with Narp, such as the level of GluR expression in PV-INs or other selective protein interactions. Currently, assays of native GluR4 trafficking are technically limited due to lack of appropriate antibodies, and our attempts at expressing an N-terminal-tagged GluR4 transgene resulted in similar elevated levels in both WT and *Narp*$^{-/-}$ PV-INs which were unresponsive to activity.

The observation that *Narp*$^{-/-}$ mice showed accelerated kindling to class V seizures provides insight into conditions in which Narp may contribute to the suppression of network excitability. It is notable that the baseline properties of excitatory synapses on hippocampal PV-INs in the dentate gyrus were not different in *Narp*$^{-/-}$ mice; only after MECS did we observe a change in excitatory input strength. The activity level *in vivo* was much less than in our primary cultures and this difference was consistent with a minimal role of Narp under basal conditions in the hippocampus *in vivo*. *Narp*$^{-/-}$ mice showed identical initial responses to kindling stimuli but clearly diverged in their responses as the kindling process evolved. Together, this suggests that Narp becomes part of the physiological adaptation only under conditions of intense activity, and is consistent with culture models that suggest the inability to recruit GluR4 levels to excitatory synapses on PV-INs in response to activity may underlie enhanced kindling. These studies do not exclude a role for Narp in scaling of PV-INs in physiological plasticity, since recordings of sEPSCs may not detect the small subset of Narp-associated excitatory synapses relevant for proper network function under basal conditions. Moreover, studies of *Narp* mRNA expression indicate that Narp is induced by non-epileptiform activity in models of cocaine administration[42], monocular deprivation[7], and *in vivo* LTP[7]. Because of the striking complexity of interneuron populations *in vivo* and

their importance to integrated neural function it will be compelling to assess the contribution of Narp-dependent homeostatic plasticity in broader studies of physiological plasticity and models of disease.

Methods

Animals

All wild-type and *Narp*$^{-/-}$ mice were of the genetic background C57/Bl6. The use of vertebrate animals was regulated and approved by the Johns Hopkins University Animal Care and Use Committee.

Antibodies

We used the following primary antibodies in this study: Narp rabbit polyclonal[15] (1:1,000), Parvalbumin mouse monoclonal (1:2,000, Sigma, St. Louis, MO) or goat polyclonal (1:2,000, Swant, Bellinzona, Switzerland), Calretinin mouse monoclonal (1:1,000 BD Biosciences, San Jose, CA), αCAMKII mouse monoclonal (1:1,000 Boehringer Mannheim/Roche,Indianapolis, IN), GluR2 mouse monoclonal (1:200, Chemicon/Millipore, Billerica, MA), GluR4 rabbit polyclonal (1:100, Chemicon/Millipore, Billerica, MA), NR1 mouse monoclonal (BD Pharmingen, 1:500, San Jose, CA), GAD65 mouse monoclonal (1:2,000, Chemicon/Millipore, Billerica, MA), Transferrin receptor mouse monoclonal (1:1,000, Zymed/Invitrogen, Carlsbad, CA), and PSD95 mouse monoclonal (1:500, Affinity Bioreagents/Thermo Scientific, Rockford, IL).

For immunocytochemical studies, we used fluorescent secondary antibodies (Molecular Probes/Invitrogen, Carlsbad, CA) at 1:400. We used peroxidase-conjugated secondaries (Pierce/Thermo Scientific, Rockford, IL) for western blot detection at 1:10,000

Cell culture

We plated hippocampal preparations of E17.5 WT or *Narp*$^{-/-}$ mice on 25 mm coverslips coated with poly-D-lysine (1 mg/mL in 0.1M Trizma buffer pH 8.5) at a density of 4×10^5 cells per 60 mm dish for immunocytochemistry, 1×10^6 cells per well (6-well plate) for biochemistry, and 1.5×10^6 per 60 mm dish for electrophysiology. We initially cultured neurons in Neurobasal (Invitrogen, Carlsbad, CA) media containing 5% horse serum (Hyclone/Thermo Scientific, Rockford, IL), 1% penicillin/streptomycin (Invitrogen, Carlsbad, CA), 2% Glutamax-I (Invitrogen, Carlsbad, CA), and 2% B-27 supplement (Invitrogen, Carlsbad, CA). We added Cytosine arabinoside (AraC) on DIV 4 to inhibit glial proliferation. After 7 days, we fed neurons by replacing half the media with Neurobasal media containing 1% fetal bovine serum, 1% penicillin/streptomycin, 2% Glutamax-I, and 2% B-27 supplement after which we fed neurons twice weekly.

For wild-type/*Narp*$^{-/-}$ co-culture, we dissociated and labeled either *Narp*$^{-/-}$ or wild-type hippocampal neurons with 2 μM Vybrant® CM-DiI (Invitrogen, Carlsbad, CA) for 20 minutes at 37°C. We then pelleted cells and washed them 3 times with pre-warmed growth medium prior to plating at 1.5×10^4 cells per 60 mm dish alongside unlabeled neurons of the opposing genotype, plated at 4×10^5 cells per 60 mm dish.

Immunocytochemistry

For GluR2, GluR4, and NR1 staining, we fixed DIV 14–17 cells in ice-cold methanol for 20 minutes at −20°C prior to staining. Otherwise, we fixed DIV 14–17 cells with 4% paraformaldehyde/4% sucrose in PBS for 20 minutes at 25°C followed by permeablization with 0.2% Triton-X 100 for 10 minutes at 25°C. We blocked nonspecific binding of antibodies with 10% goat serum (Colorado Serum Company, Denver, CO) in PBS. Following application of primary and secondary antibodies, we mounted coverslips with ProLong® Gold Antifade Reagent (Invitrogen, Carlsbad, CA).

For surface labeling of Narp, we incubated neurons with Narp antibody live for 20 minutes at 10°C in serum-free medium prior to fixation.

To label perineuronal nets, we added fluorescein-conjugated *Vicia villosa* agglutinin (2 μg/mL, Vector Laboratories, Burlingame, CA) to neurons for 10 minutes prior to fixation. For chondroitinase ABC treatments, we incubated cells in 0.2 U chondroitinase ABC (Sigma, St. Louis, MO) for 48 hours prior to fixation.

Immunohistochemistry

We anesthetized mice with pentobarbitol prior to perfusion fixation with 4% paraformaldehyde. We made 40 μm free-floating sections using a VT-1000S vibratome (Leica Microsystems, Bannockburn, IL,). For Narp staining, we incubated sections in 10 mM sodium citrate buffer (pH 6) for 30 minutes at 80°C, prior to blocking in 10% goat serum, 1% BSA, and 0.3% Triton-X 100 in PBS for 1 hour and followed by overnight incubation with primary antibody at 4°C. For GluR4 staining, we incubated sections in PBS for 30 minutes at 37°C, followed by incubation with pepsin (1mg/mL, DAKO, Glostrup, Denmark) in 0.2 M HCl for 5 minutes at 37°C, prior to blocking and staining[43]. Following application of secondary antibodies, we mounted slices with ProLong® Gold Antifade Reagent (Invitrogen, Carlsbad, CA)

Biochemistry

We added Sulfo-NHS-SS-Biotin (1 mg/mL, Thermo Scientific, Rockford, IL) to high-density hippocampal neuronal cell cultures for 30 minutes at 4°C prior to quenching with 100mM glycine and solubilization in 1% Triton, 0.5% DOC, and 0.1% SDS. We sonicated lysates and mixed NeutrAvidin Agarose resin (Thermo Scientific, Rockford, IL) with total lysates overnight. We ran immunoprecipitated protein on a NuPAGE 4–12% Bis-Tris gel (Invitrogen, Carlsbad, CA), transferred onto PVDF membrane (Thermo Scientific, Rockford, IL), and visualized with chemiluminescence (Thermo Scientific, Rockford, IL).

Real-Time PCR

We isolated total RNA from treated or untreated high-density hippocampal neuronal cell cultures using TRIzol® Reagent (Invitrogen, Carlsbad, CA). We performed reverse-transcription of the RNA using a Thermoscript™ RT-PCR system (Invitrogen, Carlsbad, CA). The forward and reverse primer sequences used for amplification were 5′-CTCCGCACAAATGTGTCTAAC-3′ and 5′-CTTCACAGGTCTCCACAGGC-3′, respectively, which yielded a 844 bp product. We set up reactions using an RT^2 SYBR®

Green qPCR Master Mix (SABiosciences, Frederick, MD) and carried out amplification and analysis using an iCycler iQ Real-Time PCR System (Bio-Rad Laboratories, Hercules, CA).

Image acquisition and analysis

We captured Z-stacks of each neuron with a Zeiss LSM 510 confocal microscope at 0.5 μm intervals, 1024×1024 pixels, 4-frame averaging, and 8-bit color without binning. Prior to quantification, we made maximum intensity projections of each neuron. We selected puncta, with an intensity above a set threshold, and residing on primary dendrites within 100 μm from the soma, for quantification. We measured puncta using ImageJ (NIH) imaging software and performed all statistics using Prism® software (GraphPad, La Jolla, CA). We expressed all values as mean ± s.e.m. We used Student's t-test with Welch's correction for all statistical comparisons between any two groups. Otherwise, for comparisons between multiple groups, we used nonparametric one-way ANOVA tests with Bonferroni analysis. We regarded $P < 0.05$ as statistically significant.

Culture Electrophysiology

We performed whole-cell patch-clamp recordings from high density (1.5×10^6 cells/ 60 mm culture dish) hippocampal cultures at DIV 14–17. To isolate AMPAR-mediated mEPSCs, we continuously perfused neurons with 30–32°C artificial cerebral-spinal fluid (aCSF) at a flow rate of 2 ml/min. The composition of aCSF was as follows (in mM): 124 NaCl, 2.5 KCl, 2.5 $CaCl_2$, 1.3 $MgCl_2$, 1 NaH_2PO_4, 26.2 $NaHCO_3$, and 10 glucose equilibrated with 95% O_2 and 5% CO_2. We adjusted the osmolarity of aCSF to 300 ± 5 mOsm and pH to 7.4. The pipette solution consisted of the following (in mM): 100 K-gluconate, 0.6 EGTA, 5 $MgCl_2$, 8 NaCl, 2 Na-ATP, 0.3 Na-GTP, and 40 HEPES. We adjusted this solution to 290 ± 5 mOsm and pH to 7.2. We pulled patch pipettes from borosilicate glass (4–5 MΩ) using a horizontal puller (Sutter Instruments, Novato, CA). We visually identified PV-INs via binding of fluorescein-tagged *Vicia villosa* agglutinin, then confirmed their fast-spiking, non-accommodating action potentials following somatic current injection[25]. We monitored passive properties of voltage clamped neurons throughout the experiments. Uncompensated series resistance (R_s) was ∼10–13 MΩ and in the event of a change in either R_s or input resistance (R_i) >15% during the course of a recording, we excluded the data from the set. We acquired mEPSCs through a MultiClamp 700B amplifier (Molecular Devices, Sunnyvale, CA), filtered at 2 kHz, and digitized at 10 kHz using a Digidata 1332A. We recorded data continuously only after allowing the cell to stabilize for 10 minutes. We acquired sweeps of 15 s with zero latency until we recorded a sufficient number of events (a minimum of 3 and no longer than 10 min). For mEPSC recording, bath solution contained both 1 μM TTX and 10 μM GABAzine to block action potential-dependent EPSCs and $GABA_A$ receptors, respectively. We manually detected mEPSCs with MiniAnalysis software (Synaptosoft Inc., Decatur, GA) by setting the amplitude threshold to RMS × 3 (usually 8 pA). Once we collected a minimum of 200 events from a neuron, we measured the amplitude, frequency, rise time (time to peak), decay time (10%–90%), and passive properties. We then averaged data from each group, and performed statistical comparison by the independent t-test, ANOVA. We purchased all drugs from Tocris (Ellisville, MO) except for TTX (Ascent Scientific LLC, Princeton, NJ).

Slice Electrophysiology

We prepared hippocampal slices (300–350 μm thick) from 3–4 week old WT and *Narp*$^{-/-}$ mice as described previously[44]. We dissected control and MECS-administered mouse littermates and interleaved recordings from slices obtained from each mouse. We anesthetized mice with isoflurane, and dissected the brain in ice-cold saline solution (in mM): 130 NaCl, 24 $NaHCO_3$, 3.5 KCl, 1.25 NaH_2PO_4, 1 $CaCl_2$, 5.0 $MgCl_2$, and 10 glucose, saturated with 95% O_2 and 5% CO_2, pH 7.4. We cut transverse slices using a VT-1000S vibratome (Leica Microsystems, Bannockburn, IL) and incubated them in the above solution at 35°C for 30 minutes following which we kept them at room temperature until use. We transferred slices to a recording chamber and perfused them (3–5 ml/min, 32–35°C) with extracellular solution (in mM): 130 NaCl, 24 $NaHCO_3$, 3.5 KCl, 1.25 NaH_2PO4, 2.5 $CaCl_2$, 1.5 $MgCl_2$, 10 glucose, 0.05 ± dl-AP5, and 0.005 bicuculline methobromide saturated with 95%O_2/5%CO_2, pH 7.4. We targeted putative PV-INs in the dentate gyrus visually identified within the first 100 μm of slices using a 40× objective and IR-DIC video microscopy (Zeiss Axioskop) for whole-cell recording using a multiclamp 700A amplifier (Axon Instruments, Foster City, CA). We filled recording electrodes (3–5 MΩ) pulled from borosilicate glass (WPI, Sarosota, FL) with (in mM): 130 K-gluconate, 5 KCl, 0.6 EGTA, 2 $MgCl_2$, 2 Na_2ATP, 0.3 GTPNa, and 10 HEPES, pH 7.2–7.3, 290mOsm. We routinely added biocytin (0.2%) to the recording electrode solution to allow *post hoc* morphological processing of recorded cells for confirmation of basket cell anatomy using fluorescently conjugated avidin to visualize the biocytin-filled cell (Supplementary Fig. 6d,e). In some cases, we also processed slices for PV immunoreactivity. We rigorously monitored uncompensated series resistance, 5–15 MΩ, and discarded recordings if changes of >10% occurred. We performed data acquisition and analysis with PC computer equipped pClamp 9.2 (Axon Instruments, Foster City, CA). We monitored firing properties of recorded cells in current clamp mode by delivery of electrotonic current injections through the recording pipette with the resting membrane potential biased to approximately −60 mV, and monitored sEPSC in voltage clamp mode at a holding potential of −60 mV. All cells included for analysis exhibited fast spiking behavior, and basket cell anatomy (Supplementary Fig 6d,e). We detected sEPSCs and analyzed them offline in Clampfit using a template event detection strategy for 30 s of gap-free recording for each cell. For each recorded cell, we averaged all events collected and used this average sEPSC to determine the amplitude, 10–90% rise time, and decay time constant (monoexponential fit). We used Student's t-test or Kolmogorov-Smirnov (K-S) tests to evaluate significance as indicated.

MECS administration

We administered MECS to 3–4 week old WT or *Narp*$^{-/-}$ mice, 12–16 hours prior to obtaining slices for electrophysiology, using a 7801 ECT unit (Ugo Basile, Comerio, Italy) (100 pulses/second, 0.4 ms pulse width, 1 second shock duration). We initially gave mice 6 mA current with successive 2 mA current increases until we observed tonic hindlimb extension[45].

Amygdala kindling procedure

We placed adult mice (3–4 months old) in a stereotaxic apparatus and anesthetized them with 2% isoflurane. We lowered a bipolar, insulated stainless-steel stimulating-recording electrode (PlasticsOne, Roanoke, VA) into the right basolateral nucleus of the amygdala (1.2 mm posterior, 2.9 mm lateral, 4.6 mm ventral) and placed a ground electrode (i.e., a jeweler's screw) in the skull over left frontal cortex. We used dental acrylic to secure the electrodes according to standard chronic methods. After a week-long recovery following surgery, we focally stimulated awake mice in the amygdala twice daily (5 days per week) with a one second train of 60 Hz biphasic constant current 1 ms square wave pulses[46]. We determined the AD threshold by a standard protocol designed to identify the minimum current necessary to evoke ADs (100–1100 μA). We scored induced seizures by standard behavioral classes as follows: (1) behavioral arrest, eye closure, vibrissae twitching, sniffing; (2) facial clonus and head bobbing; (3) forelimb clonus; (4) rearing with continued forelimb clonus; and (5) rearing with a loss of motor control and falling[47]. We evoked repeated ADs until each mouse experienced three Class V seizures and were considered fully kindled.

Supplementary Material

Refer to Web version on PubMed Central for supplementary material.

Acknowledgments

We thank M.S. Perin for the *Narp*$^{-/-}$ mouse, R.L. Huganir (Johns Hopkins University) for antibodies to GluR1, M. Dehoff and P. Chuang for animal care, M. Papapavlou for administrative assistance, and X. Yuan, and B. Jeffries for expert technical assistance. Work in the lab of C.J.M is supported by an NIH intramural award. Work in the lab of P.F.W is supported by NIH grants PAR-02-059 and NS 39156.

Bibliography

1. Turrigiano GG, Nelson SB. Hebb and homeostasis in neuronal plasticity. Curr Opin Neurobiol. 2000; 10:358–364. [PubMed: 10851171]
2. Turrigiano GG. Homeostatic plasticity in neuronal networks: the more things change, the more they stay the same. Trends Neurosci. 1999; 22:221–227. [PubMed: 10322495]
3. Turrigiano GG, Nelson SB. Homeostatic plasticity in the developing nervous system. Nat Rev Neurosci. 2004; 5:97–107. [PubMed: 14735113]
4. Chowdhury S, et al. Arc/Arg3.1 interacts with the endocytic machinery to regulate AMPA receptor trafficking. Neuron. 2006; 52:445–459. [PubMed: 17088211]
5. Shepherd JD, et al. Arc/Arg3.1 mediates homeostatic synaptic scaling of AMPA receptors. Neuron. 2006; 52:475–484. [PubMed: 17088213]
6. Park S, et al. Elongation factor 2 and fragile X mental retardation protein control the dynamic translation of Arc/Arg3.1 essential for mGluR-LTD. Neuron. 2008; 59:70–83. [PubMed: 18614030]
7. Tsui CC, et al. Narp, a novel member of the pentraxin family, promotes neurite outgrowth and is dynamically regulated by neuronal activity. J Neurosci. 1996; 16:2463–2478. [PubMed: 8786423]
8. Xu D, et al. Narp and NP1 form heterocomplexes that function in developmental and activity-dependent synaptic plasticity. Neuron. 2003; 39:513–528. [PubMed: 12895424]
9. Dodds DC, Omeis IA, Cushman SJ, Helms JA, Perin MS. Neuronal pentraxin receptor, a novel putative integral membrane pentraxin that interacts with neuronal pentraxin 1 and 2 and taipoxin-associated calcium-binding protein 49. J Biol Chem. 1997; 272:21488–21494. [PubMed: 9261167]

10. Sia GM, et al. Interaction of the N-terminal domain of the AMPA receptor GluR4 subunit with the neuronal pentraxin NP1 mediates GluR4 synaptic recruitment. Neuron. 2007; 55:87–102. [PubMed: 17610819]
11. Cho RW, et al. mGluR1/5-dependent long-term depression requires the regulated ectodomain cleavage of neuronal pentraxin NPR by TACE. Neuron. 2008; 57:858–871. [PubMed: 18367087]
12. Bjartmar L, et al. Neuronal pentraxins mediate synaptic refinement in the developing visual system. J Neurosci. 2006; 26:6269–6281. [PubMed: 16763034]
13. Kinney JW, et al. A specific role for NR2A-containing NMDA receptors in the maintenance of parvalbumin and GAD67 immunoreactivity in cultured interneurons. J Neurosci. 2006; 26:1604–1615. [PubMed: 16452684]
14. Mi R, et al. Differing mechanisms for glutamate receptor aggregation on dendritic spines and shafts in cultured hippocampal neurons. J Neurosci. 2002; 22:7606–7616. [PubMed: 12196584]
15. O'Brien RJ, et al. Synaptic clustering of AMPA receptors by the extracellular immediate-early gene product Narp. Neuron. 1999; 23:309–323. [PubMed: 10399937]
16. Doyle S, Pyndiah S, De Gois S, Erickson JD. Excitation-transcription coupling via calcium/calmodulin-dependent protein kinase/ERK1/2 signaling mediates the coordinate induction of VGLUT2 and Narp triggered by a prolonged increase in glutamatergic synaptic activity. J Biol Chem. 2010; 285:14366–14376. [PubMed: 20212045]
17. Honig MG, Hume RI. Fluorescent carbocyanine dyes allow living neurons of identified origin to be studied in long-term cultures. J Cell Biol. 1986; 103:171–187. [PubMed: 2424918]
18. O'Brien R, et al. Synaptically targeted narp plays an essential role in the aggregation of AMPA receptors at excitatory synapses in cultured spinal neurons. J Neurosci. 2002; 22:4487–4498. [PubMed: 12040056]
19. Freund TF, Buzsaki G. Interneurons of the hippocampus. Hippocampus. 1996; 6:347–470. [PubMed: 8915675]
20. Hartig W, et al. Cortical neurons immunoreactive for the potassium channel Kv3.1b subunit are predominantly surrounded by perineuronal nets presumed as a buffering system for cations. Brain Res. 1999; 842:15–29. [PubMed: 10526091]
21. Hartig W, Brauer K, Bruckner G. Wisteria floribunda agglutinin-labelled nets surround parvalbumin-containing neurons. Neuroreport. 1992; 3:869–872. [PubMed: 1421090]
22. Kosaka T, Heizmann CW. Selective staining of a population of parvalbumin-containing GABAergic neurons in the rat cerebral cortex by lectins with specific affinity for terminal N-acetylgalactosamine. Brain Res. 1989; 483:158–163. [PubMed: 2565147]
23. Bruckner G, et al. Acute and long-lasting changes in extracellular-matrix chondroitin-sulphate proteoglycans induced by injection of chondroitinase ABC in the adult rat brain. Exp Brain Res. 1998; 121:300–310. [PubMed: 9746136]
24. Geiger JR, et al. Relative abundance of subunit mRNAs determines gating and Ca2+ permeability of AMPA receptors in principal neurons and interneurons in rat CNS. Neuron. 1995; 15:193–204. [PubMed: 7619522]
25. Kawaguchi Y, Katsumaru H, Kosaka T, Heizmann CW, Hama K. Fast spiking cells in rat hippocampus (CA1 region) contain the calcium-binding protein parvalbumin. Brain Res. 1987; 416:369–374. [PubMed: 3304536]
26. Koh DS, Geiger JR, Jonas P, Sakmann B. Ca(2+)-permeable AMPA and NMDA receptor channels in basket cells of rat hippocampal dentate gyrus. J Physiol. 1995; 485(Pt 2):383–402. [PubMed: 7545230]
27. Reti IM, Baraban JM. Sustained increase in Narp protein expression following repeated electroconvulsive seizure. Neuropsychopharmacology. 2000; 23:439–443. [PubMed: 10989271]
28. Fuchs EC, et al. Recruitment of parvalbumin-positive interneurons determines hippocampal function and associated behavior. Neuron. 2007; 53:591–604. [PubMed: 17296559]
29. Morimoto K, Fahnestock M, Racine RJ. Kindling and status epilepticus models of epilepsy: rewiring the brain. Prog Neurobiol. 2004; 73:1–60. [PubMed: 15193778]
30. Alle H, Jonas P, Geiger JR. PTP and LTP at a hippocampal mossy fiber-interneuron synapse. Proc Natl Acad Sci U S A. 2001; 98:14708–14713. [PubMed: 11734656]

31. Maffei A, Nataraj K, Nelson SB, Turrigiano GG. Potentiation of cortical inhibition by visual deprivation. Nature. 2006; 443:81–84. [PubMed: 16929304]
32. Nissen W, Szabo A, Somogyi J, Somogyi P, Lamsa KP. Cell type-specific long-term plasticity at glutamatergic synapses onto hippocampal interneurons expressing either parvalbumin or CB1 cannabinoid receptor. J Neurosci. 30:1337–1347. [PubMed: 20107060]
33. Cardin JA, et al. Driving fast-spiking cells induces gamma rhythm and controls sensory responses. Nature. 2009; 459:663–667. [PubMed: 19396156]
34. Hensch TK. Critical period plasticity in local cortical circuits. Nat Rev Neurosci. 2005; 6:877–888. [PubMed: 16261181]
35. Gogolla N, Caroni P, Luthi A, Herry C. Perineuronal nets protect fear memories from erasure. Science. 2009; 325:1258–1261. [PubMed: 19729657]
36. Bekenstein JW, Lothman EW. Dormancy of inhibitory interneurons in a model of temporal lobe epilepsy. Science. 1993; 259:97–100. [PubMed: 8093417]
37. Lewis DA, Hashimoto T, Volk DW. Cortical inhibitory neurons and schizophrenia. Nat Rev Neurosci. 2005; 6:312–324. [PubMed: 15803162]
38. Doyle S, Pyndiah S, De Gois S, Erickson JD. Excitation-transcription coupling via CaMK/ERK signaling mediates the coordinate induction of VGLUT2 and Narp triggered by a prolonged increase in glutamatergic synaptic activity. J Biol Chem.
39. Lin Y, et al. Activity-dependent regulation of inhibitory synapse development by Npas4. Nature. 2008; 455:1198–1204. [PubMed: 18815592]
40. Emsley J, et al. Structure of pentameric human serum amyloid P component. Nature. 1994; 367:338–345. [PubMed: 8114934]
41. Frischknecht R, et al. Brain extracellular matrix affects AMPA receptor lateral mobility and short-term synaptic plasticity. Nat Neurosci. 2009; 12:897–904. [PubMed: 19483686]
42. Berke JD, Paletzki RF, Aronson GJ, Hyman SE, Gerfen CR. A complex program of striatal gene expression induced by dopaminergic stimulation. J Neurosci. 1998; 18:5301–5310. [PubMed: 9651213]
43. Watanabe M, et al. Selective scarcity of NMDA receptor channel subunits in the stratum lucidum (mossy fibre-recipient layer) of the mouse hippocampal CA3 subfield. Eur J Neurosci. 1998; 10:478–487. [PubMed: 9749710]
44. Pelkey KA, Lavezzari G, Racca C, Roche KW, McBain CJ. mGluR7 is a metaplastic switch controlling bidirectional plasticity of feedforward inhibition. Neuron. 2005; 46:89–102. [PubMed: 15820696]
45. Cole AJ, Abu-Shakra S, Saffen DW, Baraban JM, Worley PF. Rapid rise in transcription factor mRNAs in rat brain after electroshock-induced seizures. J Neurochem. 1990; 55:1920–1927. [PubMed: 2230801]
46. Sayin U, Osting S, Hagen J, Rutecki P, Sutula T. Spontaneous seizures and loss of axo-axonic and axo-somatic inhibition induced by repeated brief seizures in kindled rats. J Neurosci. 2003; 23:2759–2768. [PubMed: 12684462]
47. Sloviter RS. Permanently altered hippocampal structure, excitability, and inhibition after experimental status epilepticus in the rat: the “dormant basket cell” hypothesis and its possible relevance to temporal lobe epilepsy. Hippocampus. 1991; 1:41–66. [PubMed: 1688284]

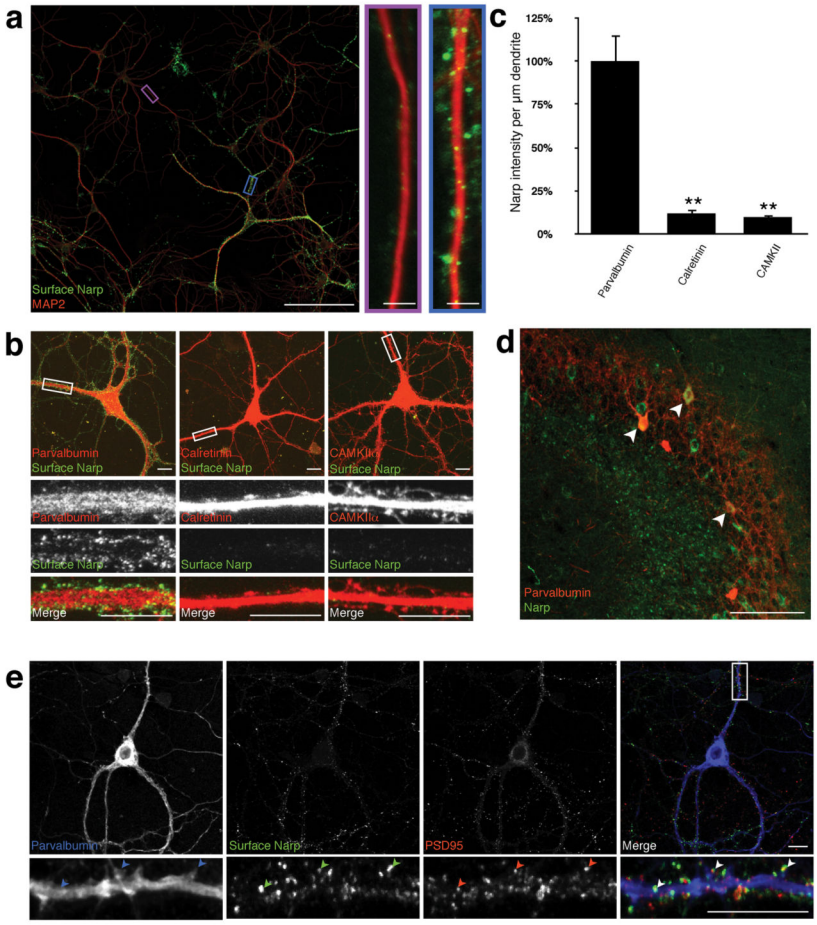

Figure 1.

Narp expression is highly enriched at excitatory synapses on PV-INs. **(a)** Representative image of hippocampal neuronal cultures stained with Narp (green) and the neuronal dendritic marker MAP2 (red). Inset: dendrite from a neuron with very little detectable surface Narp (purple border) and a dendrite from a neuron with an accumulation of surface Narp (blue border). Scale bars represent 100 µm and 5 µm (inset) **(b)** Cultured hippocampal neurons live-labeled with an antibody against Narp prior to immunostaining against cell type-specific markers PV (left), Calretinin (middle), or CAMKIIα (right). Scale bars represent 10 µm. **(c)** Summary of the data shown in **b.** Narp intensity per µm dendrite for each cell type was normalized to PV expressing neurons (PV, 100% ± 19.41%, n = 14 cells; Calretinin, 11.84% ± 3.00%, n = 15 cells; CAMKIIα, 9.72% ± 2.36%, n = 15 cells). Statistical analysis was performed using a nonparametric one-way ANOVA test. ** $P < 0.01$ vs Parvalbumin group. Error bars represent s.e.m. **(d)** Immunohistochemical staining for PV (red) and Narp (green) in the CA3 region of the hippocampus. Scale bar represents 100 µm. **(e)** Cultured hippocampal neurons were live-labeled with Narp antibody prior to immunostaining against PV and the excitatory post-synaptic marker PSD95. Arrows indicate co-localized punctae. Scale bars represent 10 µm.

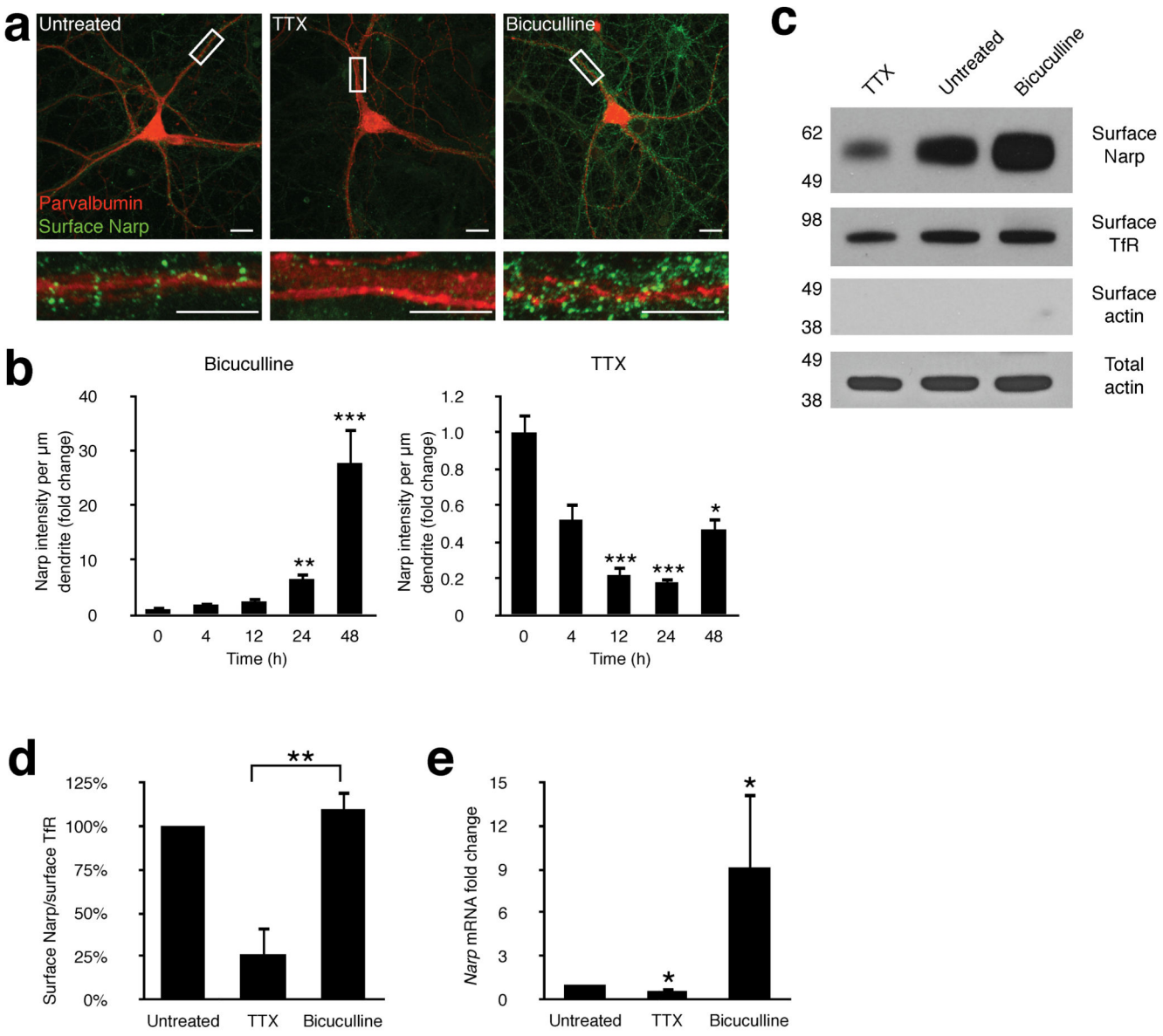

Figure 2.

Narp expression on PV-INs is dynamically regulated by activity **(a)** Following treatment for 48 hours with either 1 µM TTX (middle), control (left), or 40 µM bicuculline (right), cultured neurons were immunostained for PV and surface Narp. Scale bars represent 10 µm (top) and 5 µm (bottom). **(b)** Time course of the data shown in **a**. Narp intensity per µm dendrite after bicuculline (left) or TTX (right) treatment was normalized to 0 hour (untreated) group (Bicuculline: 0h, 100% ± 8.54%, n = 35 cells; 4h, 187.4% ± 45.47%, n = 15 cells; 12h, 241.4% ± 85.93%, n = 15 cells; 24h, 653.6% ± 126.5%, n = 15 cells; 48h, 2,770% ± 633.2%, n = 35 cells. TTX: 0h, 100% ± 10.61%, n = 35 cells; 4h, 52.27% ± 9.51%, n = 15 cells; 12h, 22.00% ± 4.58%, n = 15 cells; 24h, 18.03% ± 2.43%, n = 15 cells; 48h, 46.96% ± 6.51%, n = 32 cells) Statistical analysis was performed using a nonparametric one-way ANOVA test. ** $P < 0.01$ and *** $P < 0.001$ vs 0h group. Error bars

represent s.e.m. **(c)** Representative western blot showing levels of surface Narp, Transferrin receptor (TfR), and Actin levels in untreated control cultures (center) and after 48 hour treatment with TTX (left) or bicuculline (right). Full-length blots are presented in Supplementary Figure 2. **(d)** Summary of the data shown in **c**. All values are presented as a ratio of surface Narp intensity/surface TfR intensity and were normalized to untreated control (Untreated, 100%, n = 3; 1 μM TTX, 26.15% ± 15.73%, n = 3; 40 μM Bicuculline, 110% ± 10.32%, n = 3). Statistical analysis was performed using a nonparametric one-way ANOVA test. ** $P < 0.01$ as indicated by bracket. Error bars represent s.e.m. **(e)** Summary of Narp RT-PCR. All Narp mRNA values are normalized to paired GAPDH mRNA values and the grouped Narp mRNA averages for each treatment are normalized to untreated control cultures and presented as a fold difference. (Untreated, 1, n = 3; 1 μM TTX, 0.57 ± 0.25, n = 3; 40 μM Bicuculline, 9.12 ± 5.18, n = 3). Statistical analysis was performed using a repeated measures ANOVA test. * $P < 0.05$. Error bars represent s.e.m.

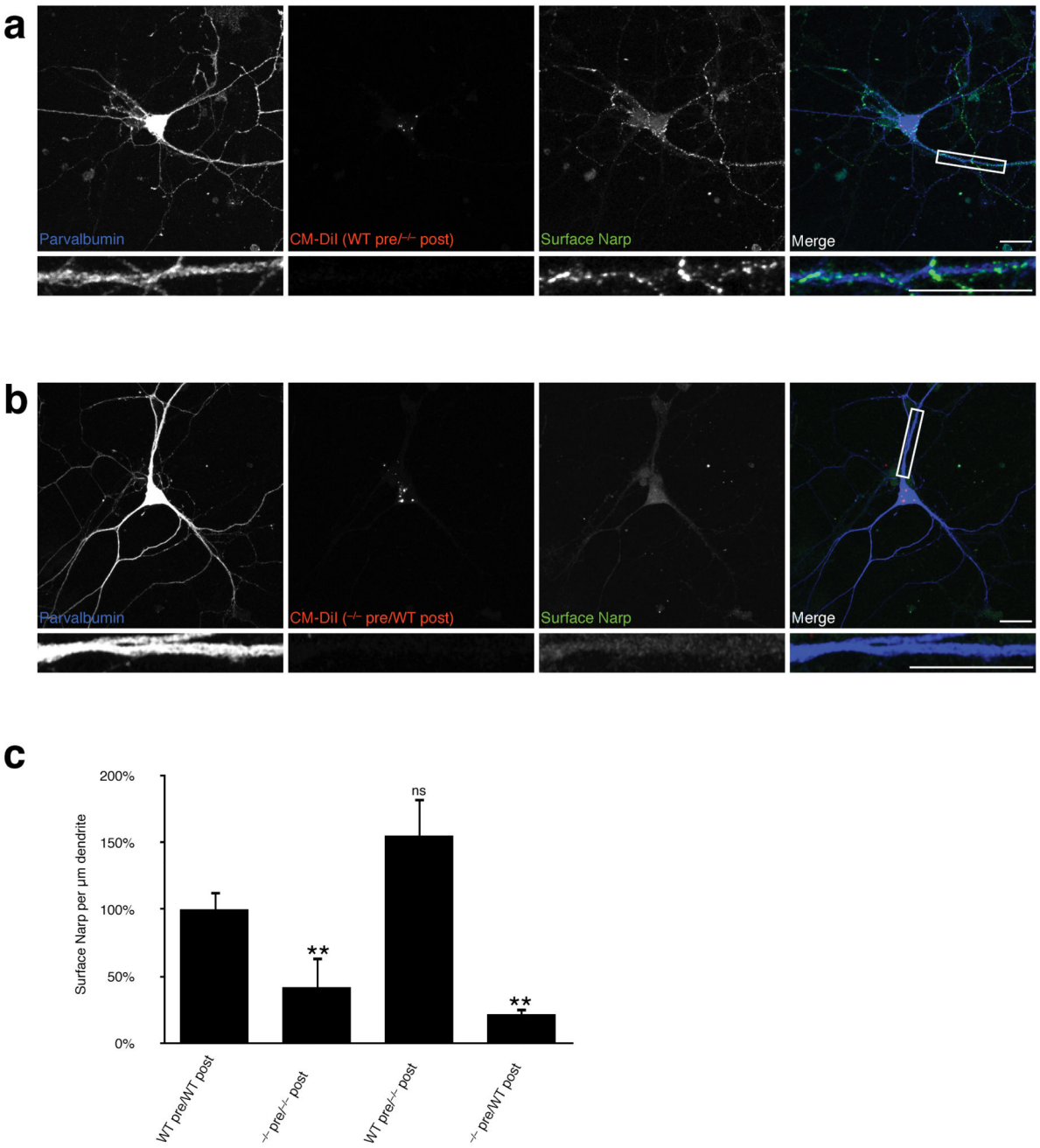

Figure 3.

Narp is derived from presynaptic neurons contacting PV-INs **(a)** Unlabeled WT hippocampal neurons plated with a small population of CM-DiI-labeled *Narp*$^{-/-}$ neurons were stained for surface Narp and Parvalbumin. **(b)** Same preparation as in **a**, but with labeled WT and unlabeled *Narp*$^{-/-}$ neurons. **(c)** Summary of the data shown in **a** and **b**. Narp intensity per µm dendrite for each condition was normalized to unlabeled WT (WT pre/WT post, 100% ± 13.65%, n = 15 cells; $^{-/-}$ pre/$^{-/-}$ post, 41.85% ± 22.53%, n = 14 cells; WT pre/$^{-/-}$ post, 155% ± 28.5%, n = 15 cells; $^{-/-}$ pre/WT post, 21.56% ± 4.76%, n = 15

cells). Statistical analysis was performed using a nonparametric one-way ANOVA test. ** $P < 0.01$ vs WT pre/WT post group.

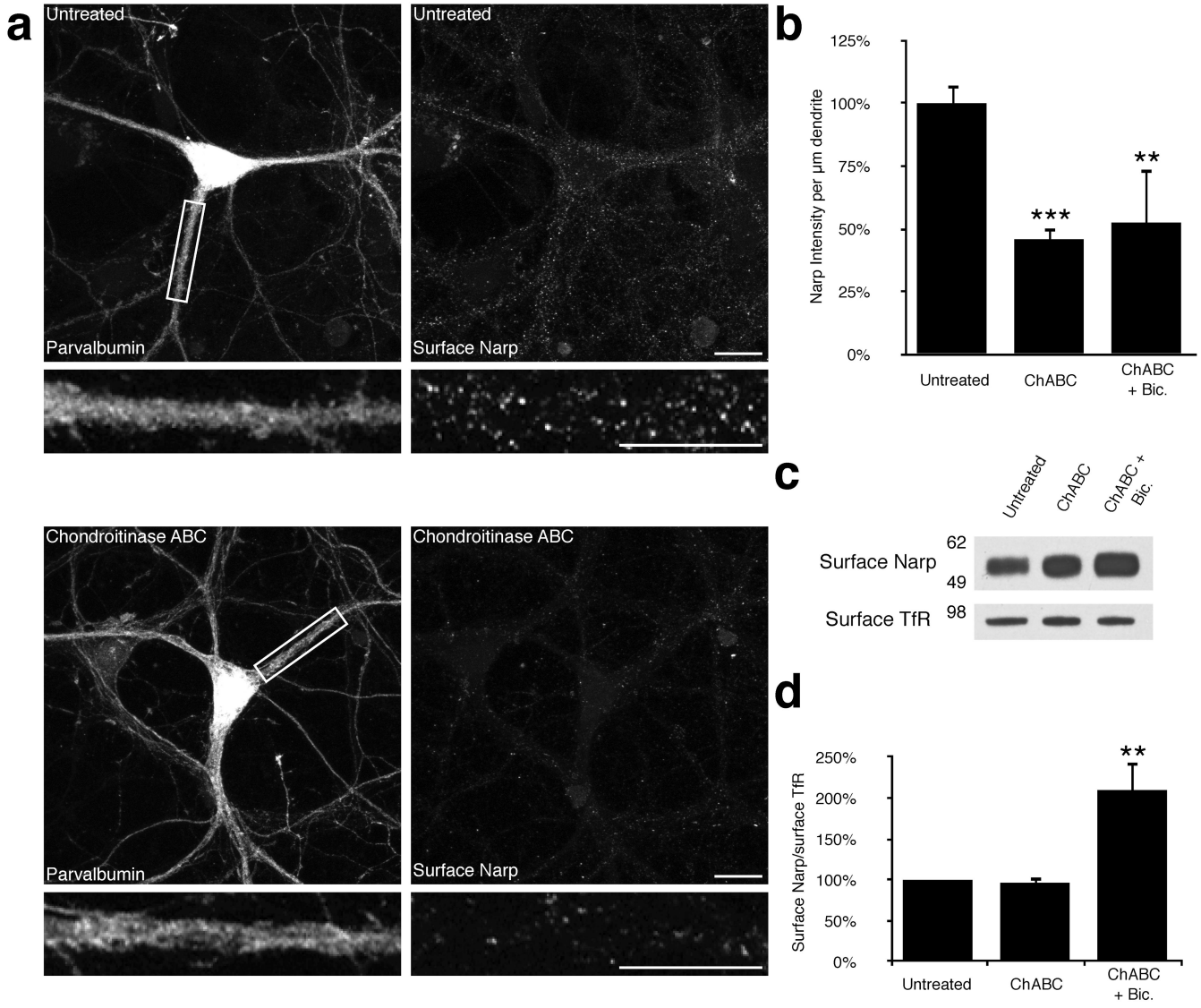

Figure 4.

Disruption of perineuronal nets results in loss of surface Narp accumulation. **(a)** (top) Untreated cultured hippocampal neurons stained for surface Narp and PV. (bottom) Representative Narp and PV immunostaining after 48 hour treatment with 0.2 U Chondroitinase ABC. Scale bars represent 10 µm. **(b)** Summary of the results seen in **a**. Narp intensity per µm dendrite for each condition was normalized to untreated control (Untreated, 100% ± 7.27%, n = 20 cells; Chondroitinase ABC, 45.83% ± 4.92%, n = 20 cells, *** $P < 0.001$ vs Untreated group; Bicuculline + Chondroitinase ABC 48 hours, 52.47% ± 4.83%, n = 19 cells). ** $P < 0.01$ vs Untreated group. Error bars represent s.e.m. **(c)** Representative western blot showing levels of surface Narp and Transferrin receptor (TfR) levels in untreated control cultures (left) and after 48 hour treatment with 0.2 U ChABC (center) or 0.2 U ChABC and 40 µM bicuculline (right). The full-length blot is presented in Supplementary Figure 2. **(d)** Summary of the data shown in **c**. All values are presented as a ratio of surface Narp intensity/surface TfR intensity and were normalized to

untreated control.(Untreated, 100%, n = 3; 0.2 U ChABC, 96.45% ± 8.18%, n = 3; 0.2 U ChABC + 40 μM Bicuculline, 210% ± 34.37%, n = 3). Statistical analysis was performed using a nonparametric one-way ANOVA test. ** $P < 0.01$ vs. Untreated group. Error bars represent s.e.m.

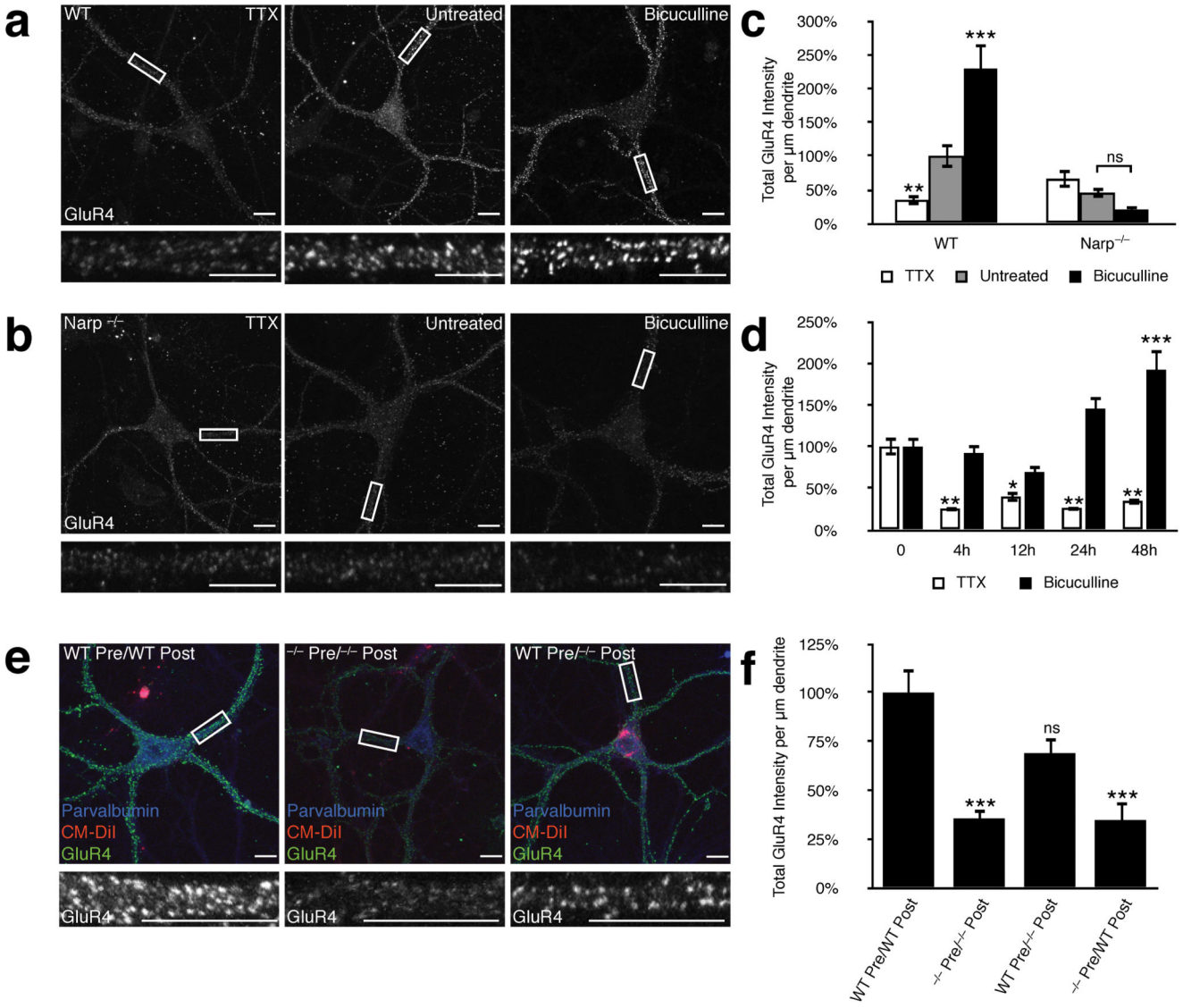

Figure 5.

Narp modulates GluR4 levels on PV-INs in an activity-dependent manner. **(a)** Representative GluR4 levels on cultured WT PV-INs in the presence of TTX (right), no treatment (middle), or bicuculline (right). Scale bars represent 10 µm (top) and 5 µm (inset). **(b)** Summary of the data shown in **a** and **c**. GluR4 intensity per µm dendrite for all treatments were normalized to WT untreated neurons (WT Untreated, 100% ± 17.71%, n = 17 cells; WT TTX, 35.10% ± 7.73%, n = 20 cells; WT Bicuculline, 229.19% ± 36.67%, n = 20 cells; *Narp*$^{-/-}$ Untreated, 45.70% ± 7.76%, n = 20 cells; *Narp*$^{-/-}$ TTX, 65.93% ± 13.24%, n = 20 cells; *Narp*$^{-/-}$ Bicuculline, 20.49% ± 6.47%, n = 20 cells) Statistical analysis was performed using a nonparametric one-way ANOVA test. *** $P < 0.001$ vs Untreated WT group or as indicated by bracket. Error bars represent s.e.m. **(c)** Same experiment as in **a** except with *Narp*$^{-/-}$ PV-INs. **(d)** Time course of PV-IN GluR4 levels during TTX (white bars) or bicuculline (black bars) treatment. GluR4 intensity per µm dendrite was normalized

to 0 hour (untreated) group (Bicuculline: 0 h, 100% ± 10.83%, n = 15 cells; 4 h, 92.35% ± 9.47%, n = 15 cells; 12 h, 69.49% ± 9.36%, n = 15 cells; 24 h, 145.4% ± 14.32%, n = 15 cells; 48 h, 192.2% ± 23.59%, n = 15 cells. TTX: 0 h, 100% ± 10.66%, n = 15 cells; 4 h, 25.77% ± 3.04%, n = 15 cells; 12 h, 40.22% ± 6.26%, n = 15 cells; 24 h, 26.64% ± 2.31%, n = 15 cells; 48 h, 35.02% ± 4.53%, n = 15 cells) Statistical analysis was performed using a nonparametric one-way ANOVA test. * $P < 0.05$, ** $P < 0.01$, and *** $P < 0.001$ vs 0 h group. Error bars represent s.e.m. **(e)** Left and right panels, unlabeled WT and labeled *Narp*$^{-/-}$ neurons were co-cultured at a ratio of 10:1. Images are representative images of an unlabeled WT (left panel) and labeled *Narp*$^{-/-}$ (right panel) neurons from the same population. Middle panel, unlabeled *Narp*$^{-/-}$ and labeled WT neurons were co-cultured at a ratio of 10:1. Shown is a representative image of an unlabeled *Narp*$^{-/-}$ neuron. Scale bars represent 10 μm **(f)** Summary of the data shown in **e**. GluR4 intensity per μm dendrite for all cell types were normalized to WT unlabeled neurons (WT pre/WT post, 100% ± 12.25%, n = 26 cells; $^{-/-}$ pre/$^{-/-}$ post, 35.57% ± 4.66%, n = 25 cells; WT pre/$^{-/-}$ post, 68.89% ± 8.52%, n = 19 cells; $^{-/-}$ pre/WT post, 34.67% ± 10.02%, n = 13 cells). Statistical analysis was performed using a nonparametric one-way ANOVA test. *** $P < 0.001$ vs. WT pre/WT post. Error bars represent s.e.m.

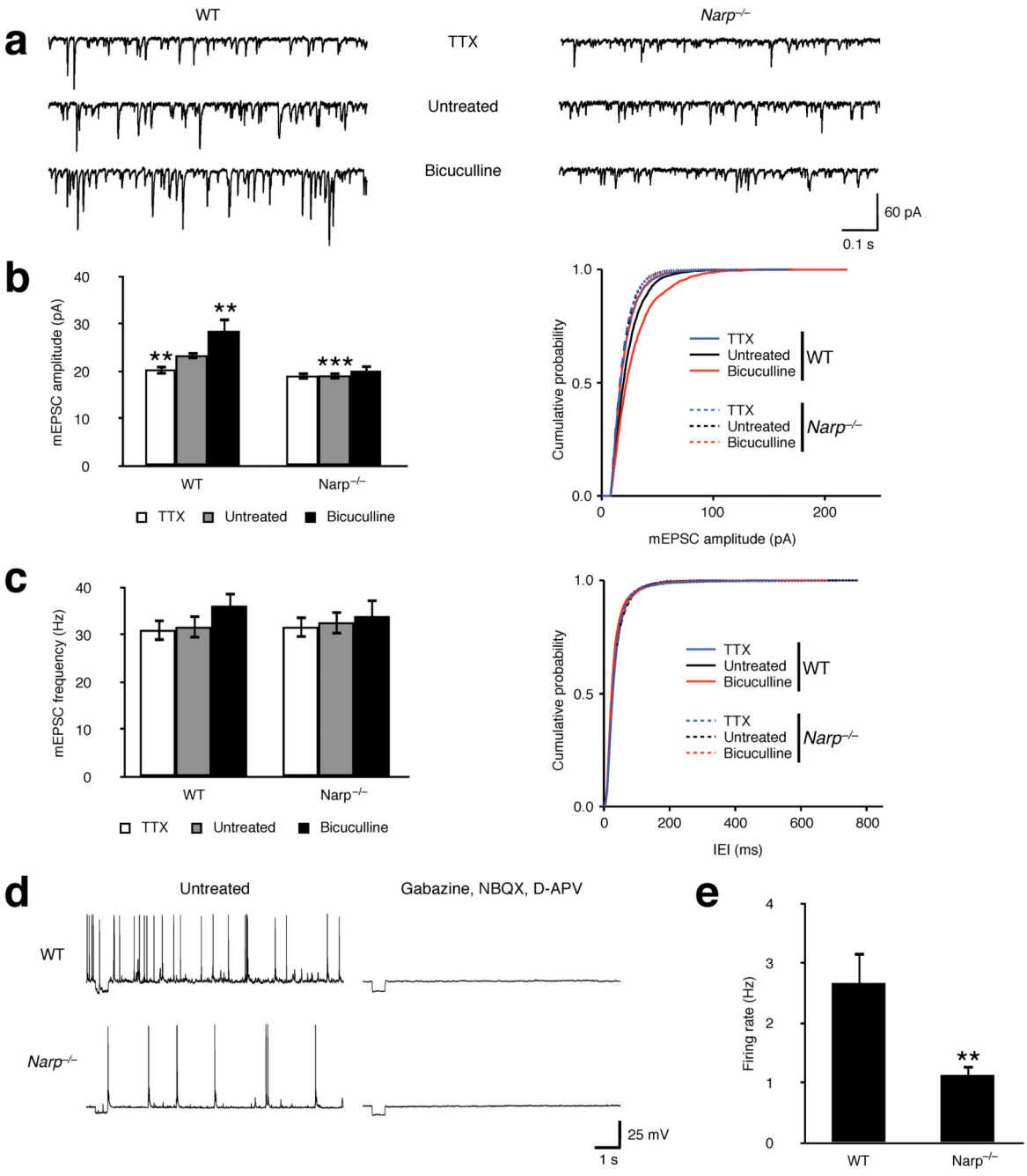

Figure 6.

Narp is required for homeostatic scaling of excitatory synaptic inputs onto PV-INs and regulates their spontaneous firing frequency. **(a)** Representative mEPSC traces of cultured WT (left) and *Narp*$^{-/-}$ (right) Parvalbumin interneurons after 48 hour treatment with TTX (top), vehicle (middle), or bicuculline (bottom). **(b)** Summary (left) and cumulative probability plot (right) of the mEPSC amplitudes obtained from all recordings similar to those shown in **a**. (WT TTX, 20.44 pA ± 1.10 pA, n = 17 cells; WT Untreated, 23.45 pA ± 0.85 pA, n = 20 cells; WT Bicuculline, 28.58 pA ± 2.68 pA, n = 15 cells; *Narp*$^{-/-}$ TTX,

19.14 pA ± 0.85 pA, n = 13 cells; *Narp*$^{-/-}$ Untreated, 19.17 pA ± 0.86 pA, n = 23 cells, *Narp*$^{-/-}$ Bicuculline, 20.17 pA ± 1.51 pA, n = 13 cells) Statistical analysis was performed using a Student's t-test. ** P < 0.01, *** P < 0.001 vs. Untreated WT group. Error bars represent s.e.m. **(c)** Summary (left) and cumulative probability plot (right) of the mEPSC frequency for all PV-INs similar to those shown in **a**. (WT TTX, 31.06 Hz ± 2.33 Hz, n = 17 cells; WT Untreated, 31.73 Hz ± 2.47 Hz, n = 20 cells; WT Bicuculline, 36.19 Hz ± 2.92 Hz, n = 15 cells; *Narp*$^{-/-}$ TTX, 31.73 Hz ± 2.33 Hz, n = 13 cells; *Narp*$^{-/-}$ Untreated, 32.66 Hz ± 2.54 Hz, n = 23 cells, *Narp*$^{-/-}$ Bicuculline, 33.99 Hz ± 3.62 Hz, n = 13 cells) Statistical analysis was performed using a Student's t-test. Error bars represent s.e.m. **(d)** Representative current clamp recordings from cultured WT (top) and *Narp*$^{-/-}$ (bottom) PV-INs showing the rate of spontaneous action potentials in the absence (left) and presence (right) of 10 μM gabazine, 10 μM NBQX, and 50 μM D-APV. **(e)** Summary of the spontaneous firing frequency of untreated PV-INs from all recordings similar to those illustrated in **d**. (WT, 2.67 Hz ± 0.51 Hz, n = 14 cells; *Narp*$^{-/-}$, 1.13 Hz ± 0.18 Hz, n = 24 cells). Statistical analysis was performed using a Student's t-test. ** P < 0.01. Error bars represent s.e.m.

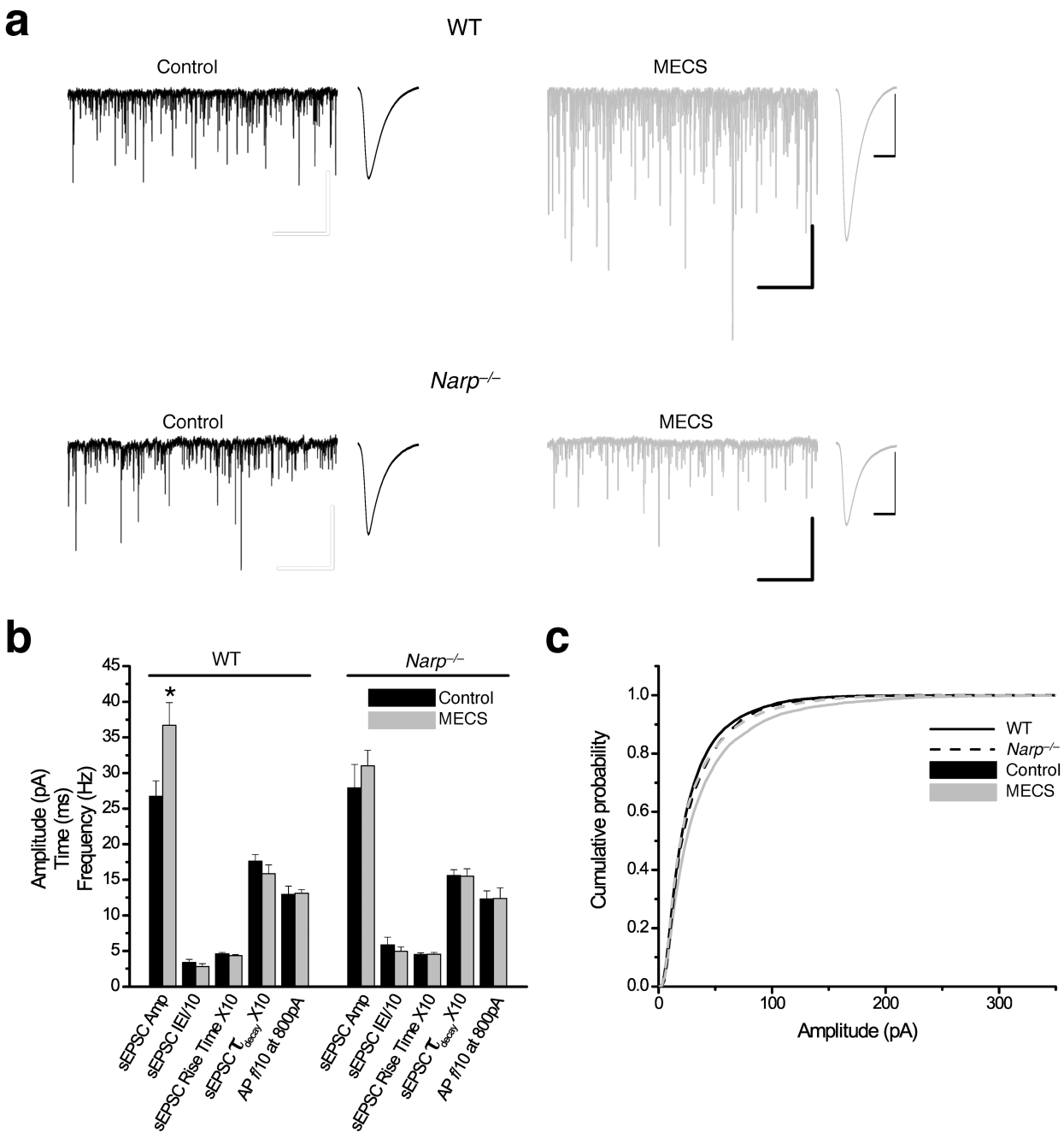

Figure 7.

Narp regulates PV-IN synaptic strength in acute hippocampal slices **(a)** Representative sEPSC records of PV-INs in acute slices from control (left) and MECS administered (right) WT (top) and *Narp*$^{-/-}$ (bottom) mice (bars 1 s/100 pA). At right of each trace is also shown the average sEPSC from each record (bars 2 ms/20 pA) **(b)** Bar chart summary of average sEPSC amplitudes, interevent intervals (IEIs), rise times, and decay time constants obtained from recordings in WT (left) and *Narp*$^{-/-}$ (right), unstimulated (black) and MECS administered (red) mice. Also shown is the group data for action potential frequency

observed in response to a sustained current injection (0.8 s/800 pA) in current-clamp mode. (WT Control sEPSC amplitude, 26.7 pA ± 2.2 pA, n = 8 cells from 4 mice; WT MECS sEPSC amplitude, 36.7 pA ± 3.2 pA, n = 7 cells from 4 mice; *Narp*$^{-/-}$ Control sEPSC amplitude, 27.9 pA ± 3.3 pA, n= 10 cells from 4 mice; *Narp*$^{-/-}$ MECS sEPSC amplitude, 31 pA ± 2.2 pA, n = 8 cells from 4 mice). Note the scaling factors (×10 or /10) for several parameters to fit on the same Y axis. Statistical analysis was carried out using a Student's t-test. * $P < 0.05$. Error bars represent s.e.m. **(c)** Cumulative probability plot for the amplitudes of all sEPSC events from all recordings obtained in WT and *Narp*$^{-/-}$ PV-INs for control and MECS conditions as indicated (for WT, $P < 0.01$ for control vs MECS). Statistical analysis was carried out using a K-S test.

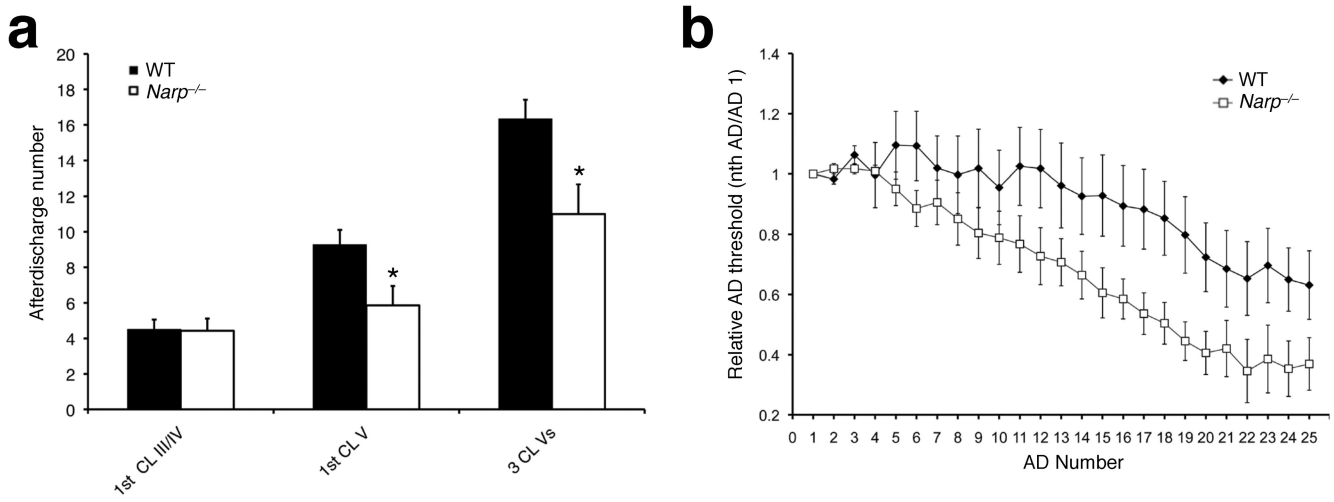

Figure 8.

Narp$^{-/-}$ mice are hypersensitive to kindling-induced seizures. **(a)** *Narp*$^{-/-}$ mice experienced Class V behavioral seizures after fewer evoked ADs than WT mice, indicating an enhanced rate of kindling progression (WT: 1st CL III/IV AD, 4.5 ± 0.5, 1st CL V AD, 9.3 ± 0.8, 3 CL V ADs, 16.3 ± 1.08, n = 22 mice; *Narp*$^{-/-}$: 1st CL III/IV AD, 4.4 ± 0.5, 1st CL V AD, 5.9 ± 0.9, 3 CL V ADs, 11.0 ± 1.6, n = 7). Statistical analysis was carried out using a one-way ANOVA and a Bonferonni test for multiple comparisons. * $P < 0.05$ vs. WT. Error bars represent s.e.m. **(b)** The relative AD threshold (i.e., the stimulation intensity required to evoke the nth AD/the stimulation required to evoke the 1st AD) decreases more rapidly for the *Narp*$^{-/-}$ mice (open squares) relative to WT mice (black diamonds) (WT AD #25, 0.63 ± 0.11, n = 24 mice; *Narp*$^{-/-}$ AD #25, 0.37 ± 0.08, n = 9 mice). Error bars represent s.e.m.